Title

Ca(2+) signaling in astrocytes from Ip3r2(-/-) mice in brain slices and during startle responses in vivo.

Journal

Nature neuroscience, 18(5)

ISSN

1097-6256

Authors

Srinivasan, Rahul
Huang, Ben S
Venugopal, Sharmila
et al.

Publication Date

2015-05-01

DOI

10.1038/nn.4001

Peer reviewed

HHS Public Access

Author manuscript

Nat Neurosci. Author manuscript; available in PMC 2015 November 01.

Published in final edited form as:

Nat Neurosci. 2015 May ; 18(5): 708–717. doi:10.1038/nn.4001.

Ca^{2+} signaling in astrocytes from *IP3R2*$^{-/-}$ mice in brain slices and during startle responses *in vivo*

Rahul Srinivasan[1,*], **Ben S. Huang**[3,*], **Sharmila Venugopal**[1], **April D. Johnston**[1], **Hua Chai**[1], **Hongkui Zeng**[6], **Peyman Golshani**[3,4,5], and **Baljit S. Khakh**[1,2,Ψ]

[1]Department of Physiology, David Geffen School of Medicine University of California Los Angeles, Los Angeles, CA 90095-1751, USA

[2]Department of Neurobiology, David Geffen School of Medicine University of California Los Angeles, Los Angeles, CA 90095-1751, USA

[3]Department of Neurology, David Geffen School of Medicine University of California Los Angeles, Los Angeles, CA 90095-1751, USA

[4]Integrative Center for Learning and Memory, David Geffen School of Medicine University of California Los Angeles, Los Angeles, CA 90095-1751, USA

[5]West Los Angeles VA Medical Center, Los Angeles, CA 90073

[6]Allen Institute for Brain Science, Seattle Washington

Abstract

Intracellular Ca^{2+} signaling is considered important for multiple astrocyte functions in neural circuits. However, mice devoid of inositol triphosphate type 2 receptors (IP3R2) reportedly lack all astrocyte Ca^{2+} signaling, but display no neuronal or neurovascular deficits, implying that astrocyte Ca^{2+} fluctuations play no role(s) in these functions. An assumption has been that loss of somatic Ca^{2+} fluctuations also reflects similar loss within astrocyte processes. Here, we tested this assumption and found diverse types of Ca^{2+} fluctuations within astrocytes, with most occurring within processes rather than in somata. These fluctuations were preserved in *IP3R2*$^{-/-}$ mice in brain slices and *in vivo*, occurred in endfeet, were increased by G-protein coupled receptor

[Ψ]Editorial and manuscript correspondence to BSK, Department of Physiology, David Geffen School of Medicine, University of California, Los Angeles, 10833 Le Conte Avenue, 53–263 CHS, Los Angeles, CA 90095–1751, Fax: 310 206 5661, Tel : 310 825 6258, bkhakh@mednet.ucla.edu.

[*]equally contributing first authors (RS and BSH)

Author contributions: RS did the molecular biology, hippocampal stereotaxic injections and most of the slice experiments with help from ADJ and HC. BSH performed all the cortical virus injections and cranial window implantations for the *in vivo* experiments. BSH and RS did the *in vivo* imaging together. SV wrote GECIquant software and RS tested it. PG shared expertise on *in vivo* calcium imaging. HZ made and shared GCaMP6f knock-in mice. RS and BSK analyzed data. BSK directed the experiments, assembled the figures and wrote the paper. All authors contributed to the final version.

Supplementary Information
11 Supplementary figures and legends
2 Supplementary tables
9 Supplementary movies
1 piece of Supplementary information providing the GECIquant script
1 piece of Supplementary information providing the GECIquant quick guide and manual

activation and by startle-induced neuromodulatory responses. Our data reveal novel Ca^{2+} fluctuations within astrocytes and highlight limitations of studies that used *IP3R2*$^{-/-}$ mice to evaluate astrocyte contributions to neural circuit function and mouse behavior.

Astrocytes are found throughout the brain and possess thousands of processes within well delineated astrocyte territories[1,2] that form the anatomical basis for interactions with neurons, other glia and blood vessels[3]. A major open question in neuroscience concerns how astrocytes contribute to the functioning of the brain and to neurological and psychiatric disorders[4]. From this perspective, much attention has focussed on the existence and physiological function(s) of astrocyte intracellular Ca^{2+} signals[5], which herein we call Ca^{2+} fluctuations.

Early studies showed that astrocytes displayed intracellular Ca^{2+} fluctuations, which were both spontaneous and triggered by neurotransmitters[6]. Subsequently, organic Ca^{2+} indicator dyes have been used extensively to study astrocyte Ca^{2+} fluctuations in brain slices and *in vivo* during various types of pharmacological and sensory stimuli (reviewed in[5,7]). In these settings, Ca^{2+} fluctuations were used in a correlative manner with simultaneous measurements from neurons or the vasculature. On the basis of such experiments, evidence indicated that astrocyte Ca^{2+} fluctuations occurred during neurotransmitter release and affected neuronal[8] and neurovascular functions[3]. Taken together, these studies suggest that astrocytes contribute to information processing and neurovascular coupling in addition to their trophic and supportive roles.

Several recent studies have questioned the physiological importance of astrocyte Ca^{2+} signaling based in large part on the use of genetically modified mice, in which Ca^{2+} fluctuations were reported to be completely absent in all astrocytes[9–11]. In such studies, the genetic deletion of inositol triphosphate type 2 receptors (IP3R2), which are known to be enriched in astrocytes[12], led to the apparent loss of all astrocyte Ca^{2+} fluctuations, but had no effect on behavioural[13], neuronal[9,10], or vascular functions[14–16], leading the authors to conclude that astrocyte Ca^{2+} fluctuations have no role(s) in these functions. However, other studies utilising similar or complementary approaches suggested that astrocyte Ca^{2+} fluctuations were involved in blood vessel and neuronal functions[17–21]. Overall, a confusing picture has emerged on astrocyte intracellular Ca^{2+} fluctuations and their physiological relevance.

We set out to test the assumption that all astrocyte Ca^{2+} fluctuations are abolished in *IP3R2*$^{-/-}$ mice. We employed fast genetically-encoded Ca^{2+} indicators[22] that can be selectively expressed in astrocytes, and not other cells[23,24], without causing astrocyte reactivity in the hippocampus[23,24], striatum[25] or cortex[16]. In these studies, astrocyte reactivity was assessed by several criteria including evaluations of GFAP staining, astrocyte proliferation and hypertrophy, and microglia activation. We also used adult mice[26] and studied astrocytes in hippocampal slices to be concordant with past work[9,10]. To avoid the complications caused by anaesthesia[27,28], we used 2-photon microscopy to study astrocytes in awake, non-anaesthetised, head-fixed mice that were free to rest or run on a treadmill. Using this paradigm, we assessed how astrocytes responded during startle responses mediated by endogenous norepinephrine release[29,30]. Finally, we employed objective, semi-

automated and standardized data analyses using newly developed software. The combination of these approaches showed that Ca^{2+} fluctuations were not abolished within astrocytes in *IP3R2*$^{-/-}$ mice as previously thought. Rather, we found a rich variety of previously unknown IP3R2 independent Ca^{2+} fluctuations within astrocyte processes that responded to pharmacological and sensory stimuli in brain slices and *in vivo*, respectively.

Results

Astrocyte spontaneous Ca^{2+} fluctuations within hippocampal slices from *IP3R2*$^{-/-}$ mice

We used adeno-associated virus (AAVs) of the 2/5 serotype and the minimal astrocyte specific *GfaABC$_1$D* promoter to express cytosolic GCaMP6f within astrocytes located in the CA1 region of the adult mouse hippocampus[23,24]. Two weeks after *in vivo* virus microinjections, we harvested hippocampal slices, identified single GCaMP6f expressing astrocytes and imaged Ca^{2+} fluctuations with confocal microscopy from wild-type (*WT*) and *IP3R2*$^{-/-}$ mice (Supplementary video 1 & 2; n = 5 mice of each genotype). GCaMP6f imaging revealed a large number of Ca^{2+} fluctuations within astrocytes, more than previously observed with organic Ca^{2+} indicator dyes[9,10,23,31,32], thus illustrating the utility of GCaMP6f[22]. In order to analyze Ca^{2+} fluctuations identically and objectively for all cells, we developed GECIquant software that permitted rapid semi-automated detection of regions of interest (ROIs) containing Ca^{2+} fluctuations (Supplementary Fig. 1; see Data analysis section for full details). GECIquant performed a series of user instigated pixel operations for maximum intensity projection, background subtraction, object thresholding, measurement of object areas, object centroids and distance of the object to the somatic centroid (Supplementary Fig. 1a–f; Supplementary Information 1). GECIquant was rigorously tested for its ability to faithfully identify, measure (Supplementary Fig. 2), trace (Supplementary Fig. 3), and track fluorescence fluctuations (Supplementary Fig. 4) using fluorescent beads, morphologically complex cells and blinking quantum dots (Supplementary Figs. 1–4). After optimization, GECIquant was used to study GCaMP6f expressing astrocytes (Supplementary Fig. 1g) that were chosen to be separated from surrounding GCaMP6f expressing astrocytes, i.e. we focussed on single cells. This was possible because of the documented sparse nature of GCaMP expression using AAV2/5 and the *GfaABC$_1$D* promoter[23,24].

In the case of *WT* mouse astrocytes expressing GCaMP6f, we could readily identify somatic Ca^{2+} fluctuations, which by definition occurred in the anatomically well defined cell body and covered an area of 80.4 ± 7.8 μm^2 (n = 109 somatic fluctuations, 15 cells, 5 mice). However, we also found numerous fluctuations in processes. One type of fluctuation within processes appeared as expanding and contracting local waves that spread between adjacent pixels; we called these “waves”. The waves spread to an area of 14.8 ± 1.4 μm^2 and displayed average centroid distances of 26.4 ± 0.7 μm from the somatic centroid (n = 837 waves, 15 cells, 5 mice). The second type of Ca^{2+} fluctuations within processes, which we called “microdomains”, were restricted in area to 0.7 ± 0.01 μm^2 and displayed average centroid distances of 29.2 ± 0.2 μm from the somatic centroid (n = 3500 microdomains, 15 cells, 5 mice). Thus, the distinction between somatic fluctuations, and waves and microdomains within processes was based on their detection using GECIquant (see Methods

for a detailed description), differences in their properties (Fig. 1), significant differences in the areas covered by the fluctuations (Supplementary Fig. 5) and their locations within astrocyte cell bodies or processes (Supplementary Fig. 6).

Once detected using GECIquant (Fig. 1a) we analyzed the numerous Ca^{2+} fluctuations in *WT* and *IP3R2*$^{-/-}$ astrocytes and quantified their basic properties (Fig. 1). We found that although the frequency (Fig. 1d), amplitude (Fig. 1e), and duration (Fig. 1f) of somatic Ca^{2+} fluctuations were significantly reduced in *IP3R2*$^{-/-}$ mice, the fluctuations were clearly not abolished (Fig. 1b–f; Supplementary video 2; $P < 0.05$ using unpaired Student's *t* tests). Moreover, we found only a subtle decrease in the frequency of waves, no change in the frequency of microdomains in processes (Fig. 1b–d), and a ~50–60% decrease in their amplitude that was accompanied by a significant increase in their duration (Fig. 1e and f; $P < 0.05$ using unpaired Student's *t* tests). Ca^{2+} waves and microdomains detected in processes were located at equivalent distances from the somata in *WT* and *IP3R2*$^{-/-}$ mice (Supplementary Fig. 5). Additionally, for the data shown in Fig. 1d–f, the number of ROIs per cell were 19 ± 2 and 196 ± 18 for waves and microdomains, respectively, for *WT* mice. The equivalent numbers for ROIs per cell were 19 ± 2 and 72 ± 6 for waves and microdomains, respectively, for *IP3R2*$^{-/-}$ mice. However, the data reported in Fig. 1d report frequency per ROI, and thus differences in the numbers of ROIs between genotypes cannot explain the differences reported in Fig 1d. Nonetheless, it should be noted that while significantly fewer microdomain ROIs were detected in *IP3R2*$^{-/-}$ in relation to *WT* mice (72 ± 6 versus 196 ± 18), microdomain ROIs were clearly not abolished. These analyses showed that Ca^{2+} signalling was not completely absent in all hippocampal astrocytes as previously reported[9–11,33]. Moreover, from a population of 15 cells from 5 *WT* and 17 cells from 5 *IP3R2*$^{-/-}$ mice, respectively we found that most Ca^{2+} fluctuations occurred in processes rather than the somata (Fig. 1). Hence, in *WT* mice the overall numbers of Ca^{2+} fluctuations in somata and processes were 4.7 ± 1.6 and 37.7 ± 8.5 fluctuations per cell per min for somata and processes, respectively. In the case of *IP3R2*$^{-/-}$ mice the equivalent numbers were 0.5 ± 0.2 and 15.6 ± 3.6 fluctuations per cell per min for somata and processes, respectively. This is a significant discovery given that past evaluations using *IP3R2*$^{-/-}$ mice have been based on measurement and quantification of somata alone[9–11,33].

To further verify our measurements, we performed one specific set of analyses to examine Ca^{2+} fluctuations within entire astrocytes by measuring the mean fluorescence intensity values for traces lasting 300 s. For this specific data set, ROIs that approximately encompassed entire astrocytes (i.e. territories) were drawn (Fig. 2a,b); note that the drawing of territory ROIs was approximate and only used for the data set in Fig. 2c. We reasoned that if Ca^{2+} fluctuations were absent in IP3R2$^{-/-}$ mice then this analysis would reveal significantly lower mean fluorescence values over time in comparison to *WT* mice, where there was an abundance of Ca^{2+} fluctuations (Fig. 1). In contrast, we found no significant differences in mean fluorescence over 300 s long traces between *WT* and *IP3R2*$^{-/-}$ mice (Fig. 2c; $P = 0.63$ with an unpaired Mann-Whitney test), suggesting that, when averaged across entire astrocytes, fluctuations in astrocyte Ca^{2+} are largely preserved in *IP3R2*$^{-/-}$ mice (Fig. 2b, c). A similar result was found when we pooled wave and microdomain fluctuations from processes (Fig. 2d). We found only subtle changes in frequency and

duration of these pooled events (Fig. 2d). We did detect a halving of the amplitude in *IP3R2*$^{-/-}$ mice (Fig. 2d; $P < 0.00001$ with an unpaired Mann-Whitney test). However, this was accompanied by an increase in the average area of pooled waves and microdomains per astrocyte in *IP3R2*$^{-/-}$ mice (Fig. 2d). The areas of the individual types of Ca^{2+} fluctuations are shown in Supplementary. Fig 5. Overall, the loss of IP3R2s resulted in significant, but incomplete loss of somatic Ca^{2+} fluctuations. In contrast, Ca^{2+} fluctuations in processes were still present, and when carefully assessed by several metrics they existed in significant numbers in *IP3R2*$^{-/-}$ mice (Figs. 1–2).

Interestingly, many Ca^{2+} fluctuations within processes were also seen in *WT* mice after depletion of intracellular Ca^{2+} stores with cyclopiazonic acid (CPA) (Supplementary tables 1 & 2; n = 10 cells from 3 mice). We next directly compared Ca^{2+} fluctuations observed in *IP3R2*$^{-/-}$ mice with fluctuations in *WT* mice after CPA. Overall these two data sets were similar, but nonidentical (Supplementary tables 1 & 2). This may suggest the existence of subtle differences in the ability of CPA and *IP3R2*$^{-/-}$ to “unmask” the signals that are not dependent on intracellular Ca^{2+} stores. However, the main point is that many signals can be observed in astrocyte processes of *WT* mice after depletion of stores with CPA, which recalls, but is not identical to, the *IP3R2*$^{-/-}$ data (Supplementary tables 1 & 2).

We next addressed the issue of whether the Ca^{2+} fluctuations we report in single astrocytes (Fig. 1) may reflect some fluctuations emanating from other nearby astrocytes also expressing GCaMP6f. This issue cannot be addressed by filling an astrocyte with a fluorescent dye via a patch pipette to demarcate its territory, because in the CA1 region the dye will spread to ~50–200 neighboring astrocytes within minutes via gap junction coupling[34–36] and thus make the task of defining the boundaries of the patched cell even more problematic. Moreover, the act of patching an astrocyte is disruptive and leads to run down of Ca^{2+} fluctuations[37]. Finally, our past experiences using this approach[32] in relation to the use of GCaMP3[23] showed that GCaMP3 was vastly superior. However, in order to address this issue we compared our original data set that was gathered from single astrocytes to a specific set of astrocytes that were selected to be completely isolated from other GCaMP6f expressing astrocytes (Supplementary Fig. 7), which was possible because of the sparse nature of GCaMP6f expression by AAV2/5[24]. We also compared both these data sets to astrocytes from offspring of GCaMP6f^{flx} mice crossed with *GLAST*-CreERT2 mice after tamoxifen induction[24]. In this genetic cross, only ~31% of astrocytes in the CA1 region express GCaMP6f and of these ~37% are easily identified as isolated, which permitted assessment of Ca^{2+} fluctuations in isolated cells (Supplementary Fig. 8). If we had overestimated the frequency of Ca^{2+} fluctuations in our original data set (Fig.1), then we would predict lower frequencies in the isolated astrocytes (from AAV2/5 injections and GCaMP6f^{flx} mice). In fact, we found no statistically significant differences in the frequency of Ca^{2+} fluctuations across these three groups (Supplementary Fig. 9). These data are entirely consistent with detailed anatomical studies showing that astrocytes have extremely well delineated territories that overlap by only ~5% among adjacent cells[1,2] and that astrocytes in the CA1 region of mice also do not possess long processes that extend beyond their individual territories[1,2].

Ca^{2+} fluctuations in astrocyte processes are partly dependent on transmembrane Ca^{2+} fluxes

The data reported in Figs 1–2 show that a component of astrocyte Ca^{2+} fluctuations are dependent on Ca^{2+} release from intracellular stores. We next explored how the Ca^{2+} fluctuations were affected by the application of nominally Ca^{2+} free buffers (Fig. 3). Application of Ca^{2+} free buffers significantly and reversibly reduced basal Ca^{2+} levels measured in astrocytes (Fig. 3a). However, Ca^{2+} free buffer applications did not significantly change the frequency of somatic Ca^{2+} fluctuations (Fig. 3b), which is consistent with the observation that somatic fluctuations were significantly reduced in the *IP3R2*$^{-/-}$ mice (Fig. 1). In contrast, for 37 and 52% of wave and microdomain ROIs located in processes, Ca^{2+} free buffers significantly and reversibly reduced the Ca^{2+} fluctuation frequency (Fig. 3c,d). The frequencies of fluctuations in the remaining 63% of wave and 48% of microdomain ROIs were not significantly affected (Supplementary Fig. 10). These data suggest that transmembrane Ca^{2+} fluxes contribute significantly to basal Ca^{2+} levels and to a detectable proportion of waves and microdomains in processes (Fig. 4). Thus, mechanistically both intracellular Ca^{2+} release (Fig. 1) and entry (Fig. 3) underlie diverse Ca^{2+} fluctuations in astrocytes. It is interesting to note that the effects of Ca^{2+} free buffer on waves and microdomains was completely reversible, i.e. the fluctuations returned to their normal levels almost exactly (Fig. 3c,d). Hence, Ca^{2+} fluctuations within processes are reproducible and stable over time.

GPCR-evoked Ca^{2+} fluctuations within astrocytes in hippocampal slices from *IP3R2*$^{-/-}$ mice

We next used endothelin (200 nM) to activate Gq-protein coupled endothelin receptors (ETRs) on astrocytes in order to elicit Ca^{2+} elevations. We chose endothelin because it was used in past studies[10] and because RNA-seq analysis shows that ETRs are enriched in astrocytes relative to neurons[12], hence minimizing the potential complication of indirect actions via neurons for our evaluations. We measured strong endothelin-evoked intracellular Ca^{2+} fluctuations in the somata in 14 out of 18 *WT* astrocytes. We quantified these data by measuring the areas under the traces before and during endothelin applications (Fig. 4a). When averaged across all 18 *WT* astrocytes, endothelin significantly elevated somatic Ca^{2+} levels (Fig. 4b; $P = 0.00487$, paired Student's *t* test). By repeating similar experiments with astrocytes from *IP3R2*$^{-/-}$ mice, we found that endothelin failed to evoke significant somatic Ca^{2+} fluctuations from a population of 23 astrocytes (Fig. 4c; $P = 0.26252$, paired Student's *t* test; Supplementary videos 3 and 4). However, it should be noted that 8 out of 23 astrocyte somata from *IP3R2*$^{-/-}$ mice responded significantly to endothelin (Fig. 4c), with the response increasing from 7.1 ± 1.9 to 74.7 ± 22.3 dF/F.s ($P = 0.0162$, paired Student's *t* test).

Next, we examined endothelin-evoked Ca^{2+} fluctuations in astrocyte processes from *WT* and *IP3R2*$^{-/-}$ mice (Fig. 4d–f) and measured significant Ca^{2+} elevations in the same proportion of cells from *WT* and *IP3R2*$^{-/-}$ mice (~50%; Fig. 3d–f; $P < 0.05$, paired Student's *t* test). This shows that *IP3R2*$^{-/-}$ mice retain GPCR-mediated Ca^{2+} signaling in astrocyte processes that is indiscernible from *WT* mice. Hence, our data do not support past work suggesting that GPCR-mediated Ca^{2+} signaling is completely abolished in *IP3R2*$^{-/-}$ mice[10]. Furthermore,

since astrocytes interact with neurons via processes, and because endothelin responses were observed in processes and not in the somata of *IP3R2*$^{-/-}$ mice, our data support the suggestion[24,38] that astrocyte somata cannot be used as a proxy measure of Ca^{2+} signaling in processes (Fig. 4a–f).

Spontaneous Ca^{2+} fluctuations in cortical astrocytes *in vivo* from WT and *IP3R2*$^{-/-}$ mice

We considered it important to assess astrocyte Ca^{2+} signaling *in vivo* to be sure that our observations with hippocampal slices were representative of signaling within intact brain. Recent studies show that cortical astrocyte somata display ongoing spontaneous Ca^{2+} fluctuations and respond with increased Ca^{2+} fluctuations during *in vivo* startle responses[29,30]. We used this experimental paradigm for our evaluations. We microinjected AAV2/5 *GfABC$_1$D GCaMP6f* virus into the visual cortex of adult mice, implanted glass cranial windows and then after 2–3 weeks of recovery, we used 2-photon microscopy to assess cortical astrocytes in fully-awake, non-anesthetized, head-fixed mice that were free to run or rest on a spherical treadmill (Fig. 5a).

We first focused on detailed analyses of somata and processes. We assessed spontaneous Ca^{2+} fluctuations within astrocytes in the visual cortex of four *WT* and four *IP3R2*$^{-/-}$ mice (during stationary periods when the mice were not in locomotion[29]). We observed spontaneous somatic fluctuations as well as waves and microdomains within processes (Supplementary videos 5 & 6), with properties that largely resembled those observed in hippocampal slices (Figs. 1–2). Compared to *WT* mice, *IP3R2*$^{-/-}$ mice displayed markedly fewer Ca^{2+} fluctuations in the somata, and these fluctuations were significantly reduced in frequency and amplitude relative to *WT*, although their durations were not significantly different (Fig. 5d–f; compared with unpaired Mann-Whitney tests). In contrast to somatic Ca^{2+} fluctuations, waves and microdomains in processes were not markedly affected. We observed only ~5% and ~40% decreases in the frequency of microdomains and waves, respectively, and no significant decreases in their amplitude or duration (Fig. 5d–f). In fact, the amplitude of microdomain Ca^{2+} fluctuations were significantly increased compared to *WT* mice (Fig. 5e). Hence, overall Ca^{2+} fluctuations were reduced largely in the somata of cortical astrocytes and were largely spared in astrocyte processes (Fig. 5). This result is apparent from Supplementary movies 5 & 6, from the representative traces of Ca^{2+} fluctuations (Fig. 5b,c) and from the average data with statistical comparisons between *WT* and *IP3R2*$^{-/-}$ mice (Fig. 5d–f). Moreover, the type and subcellular pattern of Ca^{2+} fluctuations within astrocytes was similar between hippocampal astrocytes *in vitro* and cortical astrocytes *in vivo* for both *WT* and *IP3R2*$^{-/-}$ mice. This suggests that the Ca^{2+} fluctuations were not the consequence of the method employed to study them.

We were cognizant of recent studies showing no measurable alterations in neurovascular coupling in *IP3R2*$^{-/-}$ mice[14,16,17]. Based on the assumption that all Ca^{2+} fluctuations were abolished in *IP3R2*$^{-/-}$ mice, these authors concluded that astrocyte Ca^{2+} fluctuations do not contribute to blood vessel function (but see[38]). In light of these data, we also analyzed Ca^{2+} fluctuations in astrocyte end feet from the *in vivo* data set. We found numerous Ca^{2+} fluctuations in end feet from *WT* and *IP3R2*$^{-/-}$ mice (Fig. 6a). Overall, when compared to *WT* mice, end feet Ca^{2+} fluctuations in *IP3R2*$^{-/-}$ mice displayed significant reductions in the

frequency and amplitude within individual endfeet, but showed no change in duration (Fig. 6a). Thus, overall end feet Ca^{2+} fluctuations are halved in number and reduced by ~70% in amplitude, but clearly not abolished.

Startle-evoked Ca^{2+} fluctuations in cortical astrocytes from WT and *IP3R2*$^{-/-}$ mice

Startle-evoked Ca^{2+} fluctuations that cover all astrocytes in an imaging field of view are mediated by endogenous norepinephrine release from noradrenergic fibers emanating from the locus coeruleus and acting on astrocyte α_1 adrenoceptors[29,30]. In this study, we call these "global Ca^{2+} fluctuations" to discriminate the terminology from that used for the subcellular Ca^{2+} fluctuations reported in earlier parts of this study. We next tested if cortical astrocytes of non-anesthetized awake behaving mice responded to startle, which was elicited by a gentle puff of air to the face (Supplementary video 7). *WT* and *IP3R2*$^{-/-}$ mice were exposed to a brief (3 s) air puff to the face and Ca^{2+} fluctuations were recorded in GCaMP6f expressing cortical astrocytes using 2-photon microscopy (Fig. 7a). We readily observed startle-evoked increases in global Ca^{2+} fluctuations within astrocytes from *WT* mice, which were associated with an increase in the locomotion of the mouse on the spherical treadmill (Fig. 7a–d; n = 4 mice of each genotype). Such startle-evoked global Ca^{2+} fluctuations encompassed essentially all of the astrocytes in the field of view[29] (Fig. 7a). For these analyses, we evaluated astrocyte somatic and process compartments separately before, during and after startle responses. The somata were easy to identify and process ROIs were chosen to be within ~40 μm of the cell body. However, because all astrocytes in the field of view responded to startle, it was not possible to approximately demarcate whole astrocytes like we did for the hippocampal slice experiments in Fig 2c. Hence for the *in vivo* experiments we were unable to assess Ca^{2+} fluctuations in whole astrocytes (i.e. territories) and restrict our analyses to ROIs in somata and processes.

Startle-evoked global Ca^{2+} fluctuations in cortical astrocytes are reported in Supplementary video 8. These data are presented as still frames before (0–75 s), immediately during (225–300 s) and at two subsequent time periods after the startle (300–375 and 375–450 s) in Fig. 7a,b. The exemplar traces in Fig. 7b show locomotion activity on the spherical treadmill along with representative traces for astrocyte somatic and process Ca^{2+} fluctuations. In the case of somata, fast Ca^{2+} fluctuations were observed ~3 s after startle, which recalls past work[29]. These fluctuations decreased over time in the representative traces and on average lasted ~14 ± 1 s (Fig 7a,b,c). In relation to this, the startle-evoked increase in locomotion lasted 20 ± 10 s (n = 4 mice; range of 3–70 s). Startle-evoked somatic Ca^{2+} fluctuations were completely abolished in *IP3R2*$^{-/-}$ mice (Fig. 6c, Fig. 7a), but the startle-evoked locomotion lasted 13 ± 4 s (n = 4 mice).

In contrast to somatic fluctuations, the Ca^{2+} fluctuations measured in astrocyte processes in response to startle were multiphasic. Soon after startle, the response comprised a fast component that displayed a similar time course to the somatic response (i.e. it peaked in ~3 s and lasted 13 ± 4 s). However, in processes this fast component was followed by a delayed response (late component) that leveled off at ~50 s after the startle and was maintained for the duration of the recording and returned back to baseline slowly over 5–10 mins, i.e. with a time course far in excess of the startle-evoked locomotion of 20 ± 10 s duration. The late

component of the process responses could be easily seen in the representative traces and in the average data (Fig. 7a,b,d). The differences in time course of the fast and late components of the process response (Fig. 7d), as well as the lack of the late component in the somata (Fig. 7c), suggested that the two components may be mediated by distinct mechanisms. Consistent with this, the fast component of the process response was abolished in *IP3R2*$^{-/-}$ mice (Fig. 7d). In contrast, the late component was completely unaffected in *IP3R2*$^{-/-}$ mice (Fig. 7d).

Supplementary Fig. 11 summarizes average differences and statistical comparisons (using paired Mann-Whitney tests) between *WT* and *IP3R2*$^{-/-}$ mice at three time periods relative to baseline for startle responses. Overall, the somatic response was almost completely abolished (Supplementary Fig. 11a), whereas the startle-evoked response in processes was not significantly affected at the time points examined (Supplementary Fig. 11b). These data provide compelling evidence that astrocyte physiological Ca^{2+} fluctuations persist *in vivo* within *IP3R2*$^{-/-}$ mice.

Prazosin did not inhibit startle-evoked astrocyte process Ca^{2+} fluctuations in WT or *IP3R2*$^{-/-}$ mice

We assessed the effect of the α1-adrenoceptor antagonist prazosin on startle-evoked Ca^{2+} fluctuations in *WT* and *IP3R2*$^{-/-}$ mice (Fig. 8). Cranial-window-implanted *WT* and *IP3R2*$^{-/-}$ mice expressing GCaMP6f in astrocytes were subjected to a three second air puff to the face, and baseline startle responses were recorded from cortical astrocytes (n = 4 mice of each genotype). These mice were then injected with prazosin (1 mg/kg i.p.) and 30 min later, startle responses were recorded in the same field of view of astrocytes to allow direct comparison of control *vs.* prazosin effects in the same cells (Fig. 8a). Prazosin completely inhibited startle-induced Ca^{2+} fluctuations in astrocyte somata of *WT* mice (Fig. 8b), but as expected did not alter the lack of Ca^{2+} fluctuations observed from the somata of *IP3R2*$^{-/-}$ mice (Fig. 8c). In the processes of *WT* astrocytes, prazosin selectively inhibited the fast component of the startle-evoked Ca^{2+} event with no effect on the late component (Fig. 8d). Similarly in the *IP3R2*$^{-/-}$ mice, we measured no significant effect of prazosin on the astrocyte process Ca^{2+} fluctuations or on the late component following startle. Taken together, our *in vivo* evaluations show that a novel late component of the Ca^{2+} fluctuations measured in cortical astrocytes after startle persist in *IP3R2*$^{-/-}$ mice and are not mediated by α_1-adrenoceptors or by IP3R2 receptors.

Discussion

We used state-of-the art methods to image and analyze astrocyte Ca^{2+} fluctuations with GCaMP6f within astrocytes in brain slices and *in vivo*. There are four main findings from the work. *First*, in *WT* mice the majority of Ca^{2+} fluctuations occur in astrocyte processes and not in the somata. *Second*, Ca^{2+} fluctuations are not abolished in any astrocyte compartment, and are not markedly altered in astrocyte processes of *IP3R2*$^{-/-}$ mice. *Third*, a model GPCR agonist (endothelin) reliably evoked Ca^{2+} fluctuations in the processes of astrocytes from *WT* and *IP3R2*$^{-/-}$ mice, although the somatic response was significantly reduced in *IP3R2*$^{-/-}$ mice. *Fourth*, startle-evoked Ca^{2+} fluctuations in astrocyte processes *in*

vivo consisted of two phases: an early component mediated by α_1-adrenoceptors[29,30] and a late component that was independent of α_1-adrenoceptors and IP3R2-mediated signaling.

As shown in several recent studies[23,24,29,39], GECIs are excellent tools to study astrocyte Ca^{2+} fluctuations and have shed new light on areas of the cells such as processes that have previously been difficult to explore. We have used GCaMP6f, which is as fast as organic Ca^{2+} indicator dyes[22], although this speed was not crucial to measure astrocyte Ca^{2+} fluctuations which lasted hundreds of milliseconds to seconds[24]. Evaluations have shown that bulk loading is not appropriate to study the vast majority of an astrocyte's area[32]. We suggest that the previous reliance on bulk loading of organic Ca^{2+} indicator dyes has underestimated the true extent of astrocyte Ca^{2+} signaling and missed the vast majority of fluctuations that occur within processes. This view is supported by recent studies where main astrocyte processes[32,38,40,41] and entire astrocytes[23,24] have been studied. Data gathered with organic Ca^{2+} indicator dyes has led to the erroneous conclusion that all spontaneous and GPCR-mediated Ca^{2+} signaling was abolished in hippocampal astrocytes in *IP3R2*$^{-/-}$ mice[9–11]. Because of this finding, subsequent studies have suggested that astrocyte Ca^{2+} fluctuations have no detectable role(s) in neural functions, even though these conclusions were at odds with data using different approaches[3,7,8]. However, our data show that measuring Ca^{2+} fluctuations within physiological astrocyte compartments is necessary to understand how astrocytes contribute to brain function – an aspect not addressed previously. This is analogous to the need to understand signaling within dendritic spines and nerve terminals, which are distal compartmentalized subcellular structures akin to astrocyte processes.

Our evaluations revealed that the overall pattern of Ca^{2+} fluctuations within astrocytes was similar between hippocampal astrocytes in brain slices and cortical astrocytes *in vivo* for *WT* and *IP3R2*$^{-/-}$ mice, implying that the measured Ca^{2+} fluctuations were not the consequence of the method employed to study them. Moreover, wave and microdomain Ca^{2+} fluctuations similar to those observed in *IP3R2*$^{-/-}$ mice could also be seen in *WT* mice after intracellular store depletion. Additionally, a significant proportion of wave and microdomain Ca^{2+} fluctuations were due to transmembrane Ca^{2+} fluxes. Thus, careful analysis of *WT* and *IP3R2*$^{-/-}$ mice revealed extensive Ca^{2+} fluctuations within astrocyte processes that are IP3R2 independent.

What are the relative contributions of the startle response and locomotion for the observed Ca^{2+} fluctuations? Our data show that the fast component of the Ca^{2+} fluctuations in somata and processes lasted ~14 s and thus displayed a similar duration to locomotion[29], which lasted 13–20 s. However, the late component of the Ca^{2+} fluctuations lasted far longer (> 5 min) than the 13–20 s long locomotion evoked by startle. Moreover, cortical astrocytes are directly targeted by locus coeruleus projections[29,30,42], but the relatively long (~3 s) latency between startle onset and astrocyte Ca^{2+} fluctuations in processes and somata seems too slow to be causal for the fast tens of millisecond timescale norepinephrine-mediated responses in cortical neurons[43]. It seems likely that astrocyte Ca^{2+} fluctuations may drive slow tens-of-seconds timescale changes in K^+ concentration[44], regulate blood flow[3] via Ca^{2+}-dependent phospholipase A2, control neurotransmitter uptake[45,46] or respond to the release of neuromodulators[8]. We hypothesize that the slow elevations in basal Ca^{2+} in

processes may also regulate the tonic release of D-serine[47] and hence set a prolonged time window for NMDA receptor-dependent plasticity to occur within microcircuits that had received norepinephrine as a volume transmitter. Consistent with this proposal, resting D-serine levels in cortex are regulated by astrocytes and the availability of D-serine gates synaptic potentiation[48]. In this scenario, astrocytes would function as intermediary neuromodulators, i.e. they would bridge diffuse norepinephrine volume transmission and its effects on synapses.

More generally, exploration of the signaling potential and downstream effects of astrocyte Ca^{2+} fluctuations requires the development of novel methods to abolish all types of Ca^{2+} fluctuations that we have described. As recently discussed[5], when this new method is available and rigorously validated, it may then be opportune to determine the effects of total loss of astrocyte Ca^{2+} fluctuations on blood vessels, neurons and mouse behavior. From these perspectives, rigorous biophysical models and further experiments are necessary in order to explore astrocyte Ca^{2+} signaling, and to identify the sources of the novel Ca^{2+} fluctuations we report, which include intracellular release and extracellular entry.

We conclude that the paucity of data on processes that comprise entire astrocytes has contributed to the current controversies in the field on the relevance of Ca^{2+} signaling. Our findings call for a necessary degree of caution when interpreting past studies that concluded astrocyte Ca^{2+} fluctuations had no role(s) in neuronal and blood vessel function[9,10,14–16], because those studies relied on the assumption that all Ca^{2+} signaling was abolished in IP3R2$^{-/-}$ mice[9–11]. Our data, gathered in brain slices and *in vivo*, invalidate this view and reveal a previously unknown form of astrocyte signaling that is independent of both IP3R2 and α_1-adrenoceptors and found in astrocyte processes.

Online methods

All experimental procedures were approved by the University of California Los Angeles Office for Protection of Research Subjects and the Chancellor's Animal Research Committee. All the mice were housed on a 12 hour light dark cycle with no more than five mice per cage. All of the experiments were done between 9 am and 9 pm.

Mice, molecular biology and adeno-associated virus

IP3R2$^{-/+}$ mice were obtained from Dr. Ju Chen at UCSD and maintained as a heterozygous line. Homozygotes and *WT* littermates were used for experiments when they reached age postnatal day 46–67 (P46–P67). To generate AAV2/5 capable of expressing GCaMP6f in astrocytes, we modified plasmid "pZac2.1final" (Penn Vector Core), as reported in detail in previous work[23]. Briefly, we removed the CMV promoter flanked by *BglII* and *HindIII* sites and replaced it with the minimal (<700 bp) GfaABC$_1$D astrocyte-specific promoter, which was amplified by PCR from Addgene plasmid #19974. We then cloned *GCaMP6f* into this modified pZac2.1 vector between *EcoRI* and *XbaI* sites to generate plasmids we called "pZac2.1 *GfaABC$_1$D GCaMP6f*". The fully sequenced "pZac2.1" plasmids were sent to the Penn Vector Core, which used them to generate AAV2/5 for each construct at a concentration of $<2 \times 10^{13}$ genome copies/ml (gc/ml). All our virus constructs have been deposited at Addgene in the Khakh laboratory repository for unrestricted distribution (http://

www.addgene.org/Baljit_Khakh). The plasmid for pZac2.1 *gfaABC$_1$D GCaMP6f* has an Addgene ID number of 52925. The AAV is also available for purchase from the UPenn Vector Core.

One specific experiment (Supplementary Fig. 8) utilized GCaMP6f^{flx} mice (JAX #024105) which were crossed with GLAST-Cre/ERT2 mice (JAX #012586), as described previously for GCaMP3^{flx} mice[29]. The GCaMP6f^{flx} mice were donated to JAX[49] by Dr. Hongkui Zeng (Allen Institute for Brain Sciences). All of the information on the generation and genotyping of both lines is available at JAX by searching online for the mouse identification numbers, 024105 and 012586. Once double transgenic mice were 2 months of age, they were administered 100 μl tamoxifen at 75 mg per kg of body weight once a day for 5 days by i.p. injection. Two weeks after the last injection, the mice were used to harvest brain slices exactly as described above.

Surgery and *in vivo* microinjections for hippocampal astrocyte imaging *in situ*

Postnatal day 49–63 (P49–P63) male and female *IP3R2*$^{-/-}$ and *WT* littermate mice were used. All surgical procedures were conducted under general anesthesia using continuous isoflurane (induction at 5%, maintenance at 1–2.5% vol/vol). Depth of anesthesia was monitored continuously and adjusted when necessary. After induction of anesthesia, the mice were fitted into a stereotaxic frame, with their heads secured by blunt ear bars and their noses placed into an anesthesia and ventilation system (David Kopf Instruments). Mice were administered 0.05 ml buprenorphine (0.1 mg/ml; Buprenex) subcutaneously before surgery. The surgical incision site was then cleaned three times with 10% povidone iodine and 70% ethanol. Skin incisions were made, followed by craniotomies of 2–3 mm in diameter above the left parietal cortex using a small steel burr (Fine Science Tools) powered by a high speed drill (K.1070; Foredom). Saline (0.9%) was applied onto the skull to reduce heating caused by drilling. Unilateral viral injections were performed by using stereotaxic apparatus (David Kopf Instruments) to guide the placement of beveled glass pipettes (World Precision Instruments) into the left hippocampus (2 mm posterior to bregma, 1.5 mm lateral to midline, and 1.6 mm from the pial surface). 1.5 μl AAV2/5 *GfaABC$_1$D GCaMP6f* (at 2.4 × 10^{13} gc/ml) was injected using a syringe pump (Pump11 PicoPlus Elite; Harvard Apparatus). Glass pipettes were left in place for at least 10 min. Surgical wounds were closed with single external 5–0 nylon sutures. After surgery, animals were allowed to recover overnight in cages placed partially on a low voltage heating pad. Buprenorphine was administered two times per day for up to 2 d after surgery. In addition, trimethoprim and sulfamethoxazole (40 and 200 mg, respectively, per 500 ml water) were dispensed in the drinking water for 1 week. Mice were sacrificed at 14–21 d after surgery for imaging (typically 14 d). We chose this period because generally it takes ~2 weeks to achieve GECI expression in cells by AAV infection and because of past experiences [23,24,47].

Preparation of brain slices and confocal Ca^{2+} imaging

Coronal slices of hippocampus (300 μm) were cut in solution comprising (mM): 87 NaCl, 25 $NaHCO_3$, 2.5 KCl, 1.25 NaH_2PO_4, 25 d-glucose, 75 sucrose, 7 $MgCl_2$, and 0.5 $CaCl_2$, saturated with 95% O_2 and 5% CO_2. Slices were incubated at ~34°C for 30 min and subsequently stored at room temperature in artificial cerebrospinal fluid (aCSF) comprising

(mM): 126 NaCl, 2.5 KCl, 1.3 $MgCl_2$, 10 d-glucose, 2.4 $CaCl_2$, 1.24 NaH_2PO_4, and 26 $NaHCO_3$, saturated with 95% O_2 and 5% CO_2. All other slice procedures were exactly as described previously[23]. All imaging was performed using commercially available off-the-shelf and standard confocal microscopes. In brief, cells were mostly imaged using a confocal microscope (Fluoview 300; Olympus) with a 40× water-immersion objective lens with a numerical aperture of 0.8, and a few cells were imaged with another confocal microscope (Fluoview 1000; Olympus) using the same lens. We used the 488-nm line of an Argon laser, with the intensity adjusted to 0.5–5% of the maximum output, which was 16.9 mW in the case of the Fluoview 300 and 10 mW in the case of the Fluoview 1000. The emitted light pathway consisted of an emission high pass filter (>510 nm) before the photomultiplier tube. These settings were chosen based on the known properties of GCaMPs[23]. Astrocytes were selected from the CA1 stratum radiatum region and were typically ~40 μm from the slice surface. Endothelin was applied in the bath at ~3 ml/min using a peristaltic pump. In the case of the CPA experiments, baseline movies without CPA were acquired at 1 frame per sec for 5 min. CPA was applied at 20 μM for 30 min, after which a second movie of the same cell was acquired in the presence of CPA at 1 frame per sec for 5 min. For the Ca^{2+} free experiments shown in Fig 3, the conditions were exactly as described above except that no Ca^{2+} was added to the Ca^{2+} free buffer.

Head-bar installation, virus injection, and cranial window implantation for *in vivo* imaging

Adult (P46-67) male and female *IP3R2*$^{-/-}$ mice and *WT* littermates were anesthetized with isoflurane (4% for induction, 1-1.5 % vol/vol for maintenance) and placed in a stereotaxic frame (Kopf), with body temperature kept at ~37 °C with a feedback-controlled heating pad (Harvard Apparatus). After removing the scalp and clearing the skull of connective tissues, a custom-made lightweight metal head-bar was fixed onto the skull with cyanoacrylate adhesive (Krazy Glue) and covered with black dental cement (Ortho-Jet). A circular craniotomy (3 mm diameter) was then performed above the primary visual cortex V1 (centered at -2.5 mm lateral from lambda). With the skull opened and the dura intact, the AAV2/5-*GfaABC$_1$D-GCaMP6f* virus was injected at 2 sites (1.5 μl each) near the center of the craniotomy, at a depth of 150–200 μm. After the injections, a glass cranial window consisting of a 3 mm diameter round coverslip was implanted in the craniotomy, flush with the skull surface, and sealed in place using tissue adhesive (Vetbond). The exposed skull surrounding the cranial window was then completely covered with black dental cement to build a small chamber for imaging with a water-immersion objective. After surgery, animals were returned to their home cages for 2–3 weeks for recovery and viral gene expression before subjecting to imaging experiments. Extreme care was taken to ensure that the dura experienced no damage or major bleeding before and after cranial window implantation. Mice with damaged dura or unclear window were discarded and not used for imaging experiments.

In vivo 2-photon imaging and mouse movement tracking

Two-photon laser-scanning microscopy was performed with a moveable objective microscope (Sutter MOM) using a Ti-Sapphire laser (Coherent Ultra II) at 920 nm, through a 40X 0.8 NA water-immersion objective (Olympus). The objective was mounted at a tilt of 30 degrees to the vertical axis in order to image with the light path perpendicular to the

cranial window and the cortical surface. Images were acquired using the *ScanImage* software (Vidrio Technologies)[50] and processed with *ImageJ* (NIH). Fully awake mice, without any anesthesia, were mounted on top of a spherical treadmill by securing its head-bar onto a custom-made head-bar holder under the microscope. The treadmill consisted of an 8 inch diameter Styrofoam ball resting inside another Styrofoam hollow half-sphere (Graham Sweet Studios) into which a constant stream of compressed air was blown to keep the ball afloat, allowing mice to freely run or rest on top. Images were acquired every 750 ms (1.33 Hz). To track the animals' locomotion, the treadmill motion was measured every 25 ms (40 Hz) by a custom-designed optical sensor whose signals were converted into two servo pulse analog signals (front-back and left-right) using an external PIC microcontroller. The locomotion data were acquired simultaneously with the calcium imaging data and synchronized through the scanning mirror signals. These analog signals were digitized with a NIDAQ board (National Instruments) and acquired with the WinEDR software (Strathclyde). The microscope and treadmill were encased in a light-tight box, and the animals were kept in darkness without visible visual stimuli during the imaging sessions. Before experiments, mice were acclimated to the head fixation and to resting and running on the spherical treadmill, as previously described[43].

In vivo startle induction and drug administration

Startle was induced by presenting a brief air puff to the face of the mice while the mice were resting on top of the spherical treadmill during the imaging sessions. The air puff was delivered by pressing a hand-pump air compressor (28 x 5 cm) attached to a ¼-inch PVC tubing with its opening positioned ~1 cm away from the nostril of the mice (Fig. 4a). One press of the hand pump generates a ~3 s long gentle air puff. Behavioral startle was confirmed by the locomotion induced immediately after presenting the air puff. For the prazosin administration experiments, the mice were positioned on the spherical treadmill and control/baseline images were acquired before prazosin administration. After baseline imaging, the animals were taken off the spherical treadmill and injected with prazosin (1 mg/kg i.p., Sigma) while fully awake. After injection, these mice were immediately returned to the spherical treadmill and the identical fields-of-view used for baseline imaging were found, to allow for the direct comparison of prazosin effects in the same population of astrocytes. These mice rested on the treadmill in darkness for ~30 min before imaging commenced again to record post-prazosin Ca^{2+} responses.

Ca^{2+} fluctuation detection using GECIquant and other aspects of data analysis

Detection of astrocyte regions of interest (ROI) containing Ca^{2+} fluctuations was performed in a semiautomated manner using the GECIquant program developed using the open source ImageJ analyses platform. The same procedure was followed for brain slice and *in vivo* data. The GECIquant program is implemented in Java based ImageJ script language and runs as a plugin on ImageJ. The input to GECIquant is a confocal 2D fluorescence image stack (8 or 16 or 32-bit) of arbitrary frame size, a user defined sampling rate and with time as the third dimension (t-stack). Data outputs of GECIquant include ROI intensity changes in time, ROI areas and centroid distances of each ROI from a reference ROI. Graphical outputs of GECIquant include ROI intensity kymographs and sub-stacks consisting of fluctuations.

Supplementary Information 1 provides the script and Supplementary Information 2 provides a user manual for GECIquant.

Having analyzed all the data shown in this study, we observed three distinct types of spontaneous subcellular Ca^{2+} fluctuations within astrocytes, which we describe below and then clarify how they were detected within GECIquant. We classify Ca^{2+} fluctuations as: (1) somatic fluctuations that occur within the somata (these are restricted to somata and initial segments of processes arising from somata), (2) waves that occur exclusively within astrocyte processes and display repeated wave-like expansions and contractions of Ca^{2+}, and (3) microdomain Ca^{2+} fluctuations that display highly restricted areas in astrocyte processes. These do not expand or contract as waves and remain restricted. The distinct areas covered by these three types of fluctuations are reported in the main text and in Supplementary Fig 5. In this section, we describe a semi-automated method to accurately capture regions of interest (ROIs) for somatic, wave and microdomain Ca^{2+} fluctuations within astrocytes.

After an image series was acquired (e.g. Fig. 1), the x-y axis drift in the image stacks was stabilized using the Turboreg plugin in ImageJ. All ROIs were then detected using GECIquant. A scale was first assigned to image stacks, based on the confocal digital zoom setting. For most images, we used a 3x digital zoom, which corresponds to a scale of 0.23 μm per pixel. Briefly, a temporal projection of the movie stack was thresholded and the soma was detected with an area criterion of 30 μm^2 to infinity within GECIquant. To do this, a temporal maximum intensity projection image was first generated by GECIquant from the image stack. The projection image was manually thresholded by the user with the default setting in ImageJ. Following thresholding, a polygon selection was manually drawn around the approximate astrocyte territory of interest, and the selection was added to the ImageJ ROI manager. Note that the assignment of territory was approximate and was not used for analysis except for the specific data set shown in Fig 2b. All ROIs falling within the range of 30 μm^2 to infinity inside the polygon selection were detected by GECIquant and added to the ROI manager. An area range of 30 μm^2 to infinity allowed detection of the astrocyte somata in all cases. The resulting detection was visually checked in every case.

To detect wave and microdomain ROIs, we first demarcated and deleted the soma from original image stacks using the clear selection feature in ImageJ. This was done because the increased basal fluorescence from the astrocyte soma relative to the processes prevented accurate thresholding of images for detection of ROIs within astrocyte processes. The ROI detection module in GECIquant was launched and the microdomain ROI option was selected. Microdomains and expanding wave ROIs were detected in separate analysis sessions. We used an area range of 0.5 to 4 μm^2 to detect microdomains and an area range of 5 to 2000 μm^2 for waves. These values were chosen after initial examination of the movie frames and by using several initial “best guess” test values as a guide. Other researchers who use GECIquant will also need to invest time initially to try several “best guess” values as a way to know what values will work best for the particular cell and fluctuation they are interested in measuring. The values we report here were appropriate for our experiments. For ROI detection, GECIquant generated a temporal maximum intensity projection image from the provided image stack with the deleted cell body. The projection image was manually thresholded by the user and a polygonal selection was manually drawn around the

astrocyte of interest. GECIquant automatically detected microdomain and expanding wave ROIs based on the provided area criteria and the ROIs were added to the ImageJ ROI manager. Intensity values for each ROI were extracted in ImageJ and converted to dF/F values. For each ROI, basal F was determined during 50 s periods with no fluctuations. MiniAnalysis 6.0.07 (Synaptosoft) software was used to detect and measure amplitude, half width and frequency values for the somatic, wave and microdomain transients.

We comment on how we analyzed data for the experiments shown in Fig 2. First, for the analyses shown in Fig 2c, we made approximate ROIs that encompassed whole territories and then plotted the intensity of these regions over 300 s. From these traces, we measured the mean fluorescence intensity values over the 300 s period for each cell, and then averaged these values across all cells to generate the graphs in Fig 2c for *WT* and *IP3R2*$^{-/-}$ mice. In the case of the graphs shown in Fig 2d, we pooled the individual microdomain and wave Ca^{2+} fluctuations per cell, obtained the average value per cell of these pooled fluctuations and repeated this procedure for all cells. Then we averaged across all cells to generate the graphs that are shown in Fig 2c for *WT* and *IP3R2*$^{-/-}$ mice.

Graphs were made with Origin 8.1 and the figures assembled in CorelDraw 12 (Corel Corporation). No statistical methods were used to pre-determine sample sizes but our sample sizes are similar to those generally employed in the field. Randomization and blinding was not employed. Statistical comparisons were made using unpaired non parametric Mann-Whitney or unpaired parametric Student's *t* tests as deemed appropriate after analyzing the raw data to ascertain whether they were normally-distributed using the Dallal and Wilkinson approximation to Lilliefors' method within Instat. When a statistical test was used, the precise *P* value and the test employed are reported in the text and/or figures legends. If the *P* was less than 0.00001, then it is reported as $P < 0.00001$. Otherwise, precise *P* values are provided in each case.

A methods checklist is available with the supplementary materials.

Supplementary Material

Refer to Web version on PubMed Central for supplementary material.

Acknowledgments

Most of the work was supported by the NIH (NS060677). BSK, RS and SV were also supported by NIH grants MH099559A, MH104069 and the CHDI Foundation. PG and BSH were supported by NIH MH101198-1 and Simon's Foundation Circuits Grant. The authors are grateful to current and past members of the laboratories for discussions and comments. Thanks also to Dr. MV Sofroniew for sharing equipment and to Dr. Ju Chen for sharing mice. Special thanks to Dr. Martin D. Haustein who helped with the initial testing of GECIquant and made valuable suggestions on its development. Thanks to Dr. Christopher Octeau for comments on the paper.

References

1. Bushong EA, Martone ME, Jones YZ, Ellisman MH. Protoplasmic astrocytes in CA1 stratum radiatum occupy separate anatomical domains. J Neurosci. 2002; 22:183–192. [PubMed: 11756501]
2. Wilhelmsson U, et al. Redefining the concept of reactive astrocytes as cells that remain within their unique domains upon reaction to injury. Proc Natl Acad Sci U S A. 2006 Nov 14; 103(46):17513–8. [PubMed: 17090684]

3. Attwell D, et al. Glial and neuronal control of brain blood flow. Nature. 2010; 468:232–243. [PubMed: 21068832]
4. Barres BA. The mystery and magic of glia: a perspective on their roles in health and disease. Neuron. 2008; 60:430–440. [PubMed: 18995817]
5. Khakh BS, McCarthy KD. Astrocyte calcium signals: from observations to functions and the challenges therein. Cold Spring Harb Perspect Biol. Jan 20.2015 pii: a020404. Epub ahead of print. 10.1101/cshperspect.a020404
6. Cornell-Bell AH, Finkbeiner SM, Cooper MS, Smith SJ. Glutamate induces calcium waves in cultured astrocytes: long-range glial signaling. Science. 1990; 247:470–473. [PubMed: 1967852]
7. Allen NJ. Astrocyte regulation of synaptic behavior. Annu Rev Cell Dev Biol. 2014; 30:439–463. [PubMed: 25288116]
8. Halassa MM, Haydon PG. Integrated brain circuits: astrocytic networks modulate neuronal activity and behavior. Annu Rev Physiol. 2010; 72:335–355. [PubMed: 20148679]
9. Petravicz J, Fiacco TA, McCarthy KD. Loss of IP3 receptor-dependent Ca2+ increases in hippocampal astrocytes does not affect baseline CA1 pyramidal neuron synaptic activity. J Neurosci. 2008; 28:4967–4973. [PubMed: 18463250]
10. Agulhon C, Fiacco TA, McCarthy KD. Hippocampal short- and long-term plasticity are not modulated by astrocyte Ca2+ signaling. Science. 2010; 327:1250–1254. [PubMed: 20203048]
11. Agulhon C, et al. Modulation of the autonomic nervous system and behaviour by acute glial cell Gq protein-coupled receptor activation in vivo. J Physiol. 2013; 591:5599–5609. [PubMed: 24042499]
12. Zhang Y, et al. An RNA-Sequencing Transcriptome and Splicing Database of Glia, Neurons, and Vascular Cells of the Cerebral Cortex. J Neurosci. 2014; 34:11929–11947. [PubMed: 25186741]
13. Petravicz J, Boyt KM, McCarthy KD. Astrocyte IP3R2-dependent Ca(2+) signaling is not a major modulator of neuronal pathways governing behavior. Front Behav Neurosci. Nov 12.2014 8:384. eCollection 2014. 10.3389/fnbeh.2014.00384 [PubMed: 25429263]
14. Nizar K, et al. In vivo stimulus-induced vasodilation occurs without IP3 receptor activation and may precede astrocytic calcium increase. J Neurosci. 2013; 33:8411–8422. [PubMed: 23658179]
15. Takata N, et al. Cerebral blood flow modulation by Basal forebrain or whisker stimulation can occur independently of large cytosolic Ca2+ signaling in astrocytes. PLoS One. 2013; 8(6):e66525. Print 2013. 10.1371/journal.pone.0066525 [PubMed: 23785506]
16. Bonder DE, McCarthy KD. Astrocytic Gq-GPCR-Linked IP3R-Dependent Ca2+ Signaling Does Not Mediate Neurovascular Coupling in Mouse Visual Cortex In Vivo. J Neurosci. 2014; 34:13139–13150. [PubMed: 25253859]
17. Takata N, et al. Astrocyte calcium signaling transforms cholinergic modulation to cortical plasticity in vivo. J Neurosci. 2011; 31:18155–18165. [PubMed: 22159127]
18. Chen N, et al. Nucleus basalis-enabled stimulus-specific plasticity in the visual cortex is mediated by astrocytes. Proc Natl Acad Sci U S A. 2010; 109:E2832–2841. [PubMed: 23012414]
19. Navarrete M, et al. Astrocytes mediate in vivo cholinergic-induced synaptic plasticity. PLoS Biol. 2012; 10(2):e1001259. Epub 2012 Feb 14. 10.1371/journal.pbio.1001259 [PubMed: 22347811]
20. Perez-Alvarez A, Navarrete M, Covelo A, Martín ED, Araque A. Structural and functional plasticity of astrocyte processes and dendritic spine interactions. J Neurosci. 2014; 34:12738–12744. [PubMed: 25232111]
21. Wang F, et al. Astrocytes modulate neural network activity by Ca^{2}+-dependent uptake of extracellular K+ Sci Signal. 2012; 5(218):ra26.10.1126/scisignal.2002334 [PubMed: 22472648]
22. Chen TW, et al. Ultrasensitive fluorescent proteins for imaging neuronal activity. Nature. 2013; 499:295–300. [PubMed: 23868258]
23. Shigetomi E, et al. Imaging calcium microdomains within entire astrocyte territories and endfeet with GCaMPs expressed using adeno-associated viruses. J Gen Physiol. 2013; 141:633–647. [PubMed: 23589582]
24. Haustein MD, et al. Conditions and constraints for astrocyte calcium signaling in the hippocampal mossy fiber pathway. Neuron. 2014; 82:413–429. [PubMed: 24742463]

25. Jiang R, Haustein MD, Sofroniew MV, Khakh BS. Imaging intracellular Ca^{2+} signals in striatal astrocytes from adult mice using genetically-encoded calcium indicators. J Vis Exp. Nov 19.2014 (93):e51972.10.3791/51972 [PubMed: 25490346]
26. Sun W, et al. Glutamate-dependent neuroglial calcium signaling differs between young and adult brain. Science. 2013; 339:197–200. [PubMed: 23307741]
27. Nimmerjahn A, Mukamel EA, Schnitzer MJ. Motor behavior activates Bergmann glial networks. Neuron. 2009; 62:400–412. [PubMed: 19447095]
28. Thrane AS, et al. General anesthesia selectively disrupts astrocyte calcium signaling in the awake mouse cortex. Proc Natl Acad Sci U S A. 2012; 109:18974–18979. [PubMed: 23112168]
29. Paukert M, et al. Norepinephrine controls astroglial responsiveness to local circuit activity. Neuron. 2014; 82:1263–1270. [PubMed: 24945771]
30. Ding F, et al. α1-Adrenergic receptors mediate coordinated Ca(2+) signaling of cortical astrocytes in awake, behaving mice. Cell Calcium. 2013; 54:387–394. [PubMed: 24138901]
31. Fiacco TA, et al. Selective stimulation of astrocyte calcium in situ does not affect neuronal excitatory synaptic activity. Neuron. 2007; 54:611–626. [PubMed: 17521573]
32. Reeves A, Shigetomi E, Khakh BS. Bulk loading of calcium indicator dyes to study astrocyte physiology: key limitations and improvements using morphological maps. J Neurosci. 2011; 31:9353–9358. [PubMed: 21697385]
33. Fiacco TA, Agulhon C, McCarthy KD. Sorting out astrocyte physiology from pharmacology. Annu Rev Pharmacol Toxicol. 2009; 49:151–174. [PubMed: 18834310]
34. Shigetomi E, Bowser DN, Sofroniew MV, Khakh BS. Two forms of astrocyte calcium excitability have distinct effects on NMDA receptor-mediated slow inward currents in pyramidal neurons. J Neurosci. 2008; 28:6659–6663. [PubMed: 18579739]
35. Anders S, et al. Spatial properties of astrocyte gap junction coupling in the rat hippocampus. Philos Trans R Soc Lond B Biol Sci. Oct 19.2014 369(1654):20130600.10.1098/rstb.2013.0600 [PubMed: 25225094]
36. Wallraff A, et al. The impact of astrocytic gap junctional coupling on potassium buffering in the hippocampus. J Neurosci. 2006; 26:5438–5447. [PubMed: 16707796]
37. Nett WJ, Oloff SH, McCarthy KD. Hippocampal astrocytes in situ exhibit calcium oscillations that occur independent of neuronal activity. J Neurophysiol. 2002; 87:528–537. [PubMed: 11784768]
38. Otsu Y, et al. Calcium dynamics in astrocyte processes during neurovascular coupling. Nat Neurosci. Dec 22.2014 Epub ahead of print. 10.1038/nn.3906
39. Shigetomi E, Kracun S, Sofroniew MV, Khakh BS. A genetically targeted optical sensor to monitor calcium signals in astrocyte processes. Nature Neuroscience. 2010; 13:759–766. [PubMed: 20495558]
40. Panatier A, et al. Astrocytes are endogenous regulators of basal transmission at central synapses. Cell. 2011; 146:785–798. [PubMed: 21855979]
41. Di Castro MA, et al. Local Ca2+ detection and modulation of synaptic release by astrocytes. Nat Neurosci. 2011; 10:1276–1284. [PubMed: 21909085]
42. Bekar LK, He W, Nedergaard M. Locus coeruleus alpha-adrenergic-mediated activation of cortical astrocytes in vivo. Cereb Cortex. 2008; 18:2789–2795. [PubMed: 18372288]
43. Polack PO, Friedman J, Golshani P. Cellular mechanisms of brain state-dependent gain modulation in visual cortex. Nat Neurosci. 2013; 16:1331–1339. [PubMed: 23872595]
44. Wang F, Xu Q, Wang W, Takano T, Nedergaard M. Bergmann glia modulate cerebellar Purkinje cell bistability via Ca2+-dependent K+ uptake. Proc Natl Acad Sci U S A. 2012; 109:7911–7916. [PubMed: 22547829]
45. Shigetomi E, Tong X, Kwan KY, Corey DP, Khakh BS. TRPA1 channels regulate astrocyte resting calcium and inhibitory synapse efficacy through GAT-3. Nature Neuroscience. 2011; 15:70–80. [PubMed: 22158513]
46. Muthukumar AK, Stork T, Freeman MR. Activity-dependent regulation of astrocyte GAT levels during synaptogenesis. Nat Neurosci. 2014; 17:1340–1350. [PubMed: 25151265]

47. Shigetomi E, Jackson-Weaver O, Huckstepp RT, O'Dell TJ, Khakh BS. TRPA1 channels are regulators of astrocyte basal calcium levels and long-term potentiation via constitutive D-serine release. J Neurosci. 2013; 33:10143–10153. [PubMed: 23761909]

48. Fossat P, et al. Glial D-serine gates NMDA receptors at excitatory synapses in prefrontal cortex. Cereb Cortex. 2012; 22:595–606. [PubMed: 21690263]

49. Madisen L, et al. Transgenic mice for intersectional targeting of neural sensors and effectors with high specificity and performance. Neuron. 2015; 85:942–958. [PubMed: 25741722]

50. Pologruto TA, Sabatini BL, Svoboda K. ScanImage: flexible software for operating laser scanning microscopes. Biomed Eng Online. 2003; 17;2:13.

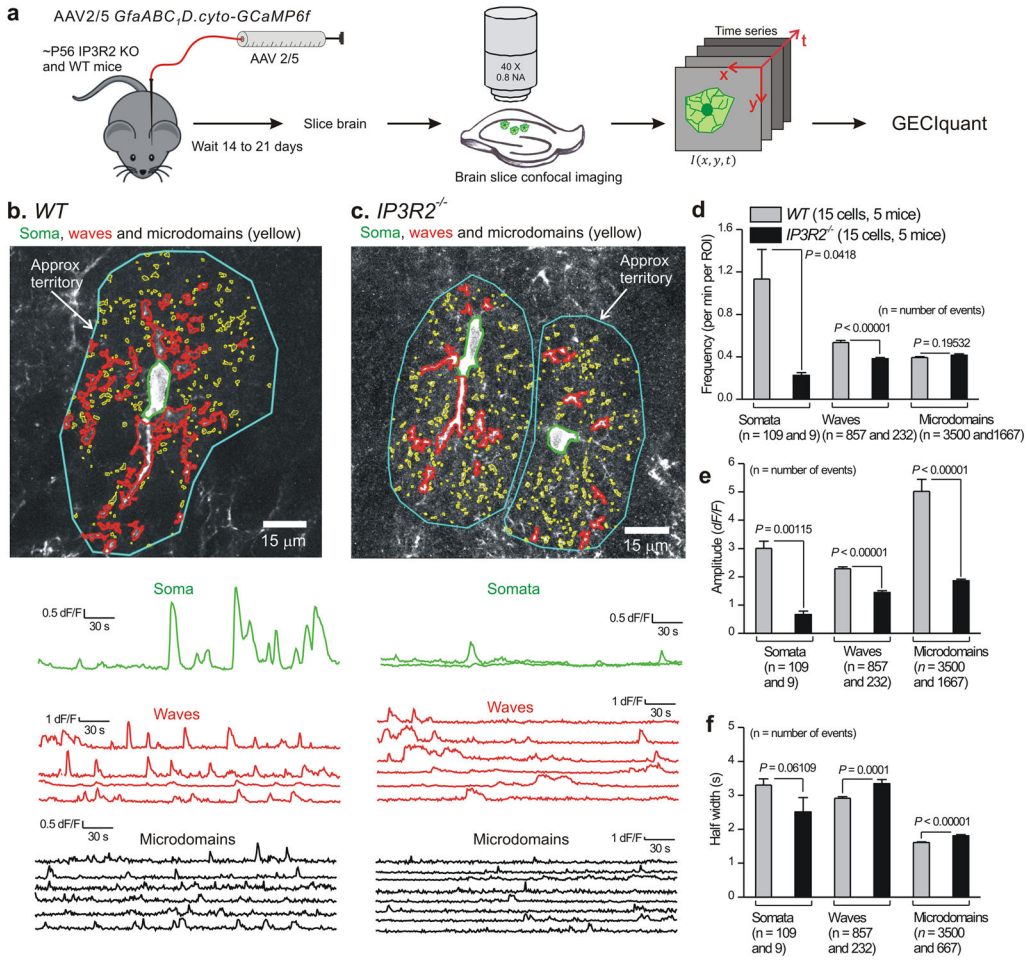

Figure 1. Ca^{2+} fluctuations in hippocampal astrocytes from WT and *IP3R2*$^{-/-}$ mice

a. Schematic illustrating the experimental approach. **b.** Representative images and traces for Ca^{2+} fluctuations measured in an astrocyte from a *WT* mouse. Three predominant types of Ca^{2+} event are demarcated: somatic fluctuations (green), waves (red) and microdomains (yellow). Approximate territory boundaries are outlined in blue, but these were not used for data analyses and are shown only for illustrative purposes. **c.** As in b, but for two astrocytes from an *IP3R2*$^{-/-}$ mouse. Representative movies are shown as Supplementary movies 1 and 2. **d–f.** Average data for Ca^{2+} fluctuation properties in *WT* and *IP3R2*$^{-/-}$ mice (n = 15 and 17 astrocytes *WT* and *IP3R2*$^{-/-}$, and 5 mice for each). For this and all other figures, statistical comparisons were made using unpaired non-parametric Mann-Whitney or unpaired parametric Student's *t* tests as deemed appropriate after analyzing the raw data (see Data analysis). The n numbers on d–f refer to the numbers of Ca^{2+} fluctuations for the *WT* and *IP3R2–/–* bars, which were averaged for frequency, amplitude and half-width across all cells in panels d–f. The data are shown as mean ± s.e.m.

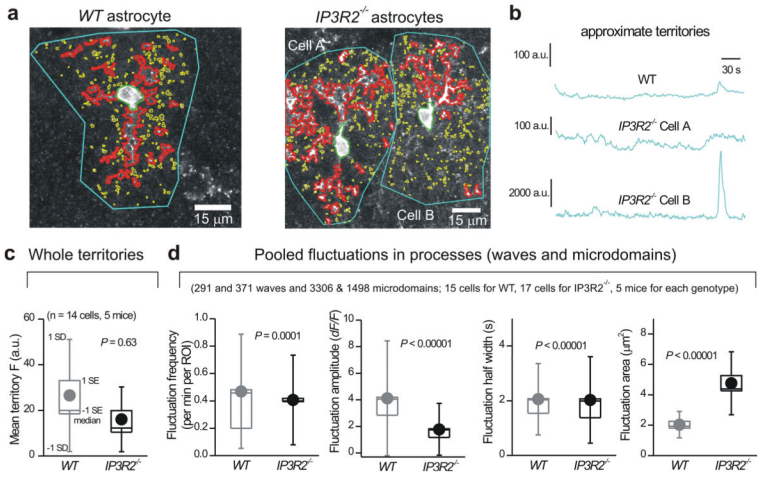

Figure 2. Ca^{2+} fluctuations within astrocyte processes are largely intact in brain slices from *IP3R2*$^{-/-}$ mice

a. Representative images of astrocytes from *WT* and *IP3R2*$^{-/-}$ mice with somatic (green), wave (red) and microdomain (yellow) compartments demarcated in different colors. Approximate territory boundaries are outlined in blue, but were only used for analyses shown in b and c. **b.** Representative traces for territory ROI fluctuations for the cells shown in a. Such traces were used to measure the average fluorescence over 300 s in panel c. Note that the drawing of the territory for this single specific data set (panel b) is approximate. **d.** Summary data for *WT* and IP3R2$^{-/-}$ mice for pooled wave and microdomain fluctuations in astrocyte processes, plotted as box and whisker plots; note that these are pooled data from microdomains and waves.

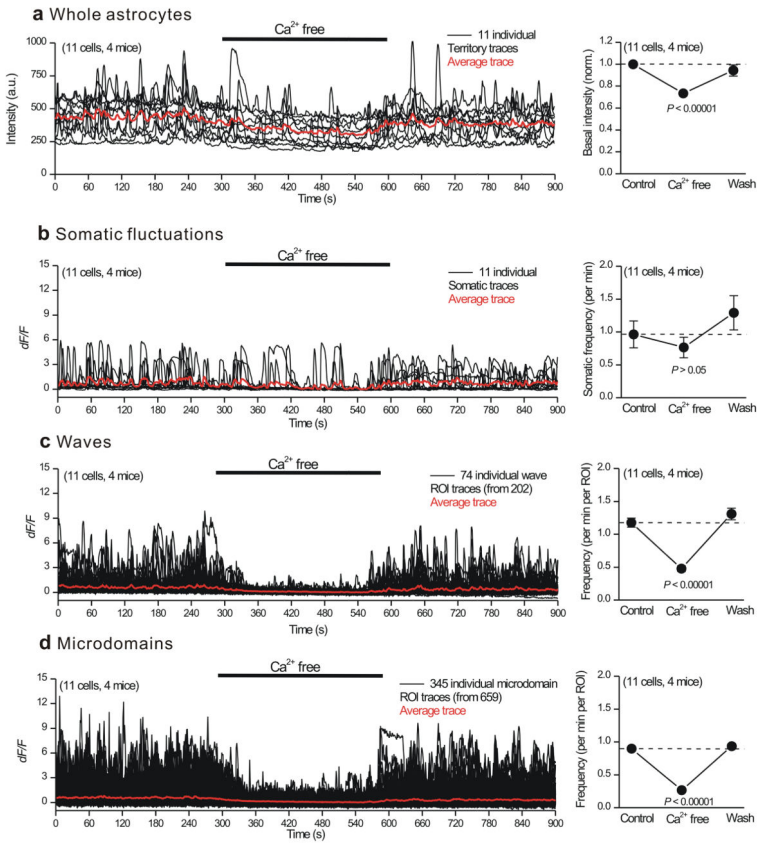

Figure 3. Effect of nominally Ca^{2+} free buffer applications on astrocyte Ca^{2+} fluctuations in WT mice

a. Traces and average data for the effect of nominally Ca^{2+} free buffers on the basal fluorescence intensity of ROIs corresponding approximately to entire astrocytes. **b–d.** As in a, but for somatic fluctuations (**b**) as well as for wave (**c**) and microdomain (**d**) fluctuations in astrocyte processes. The averages are across all cells for the ROIs indicated in each set of traces. The data are shown as mean ± s.e.m.

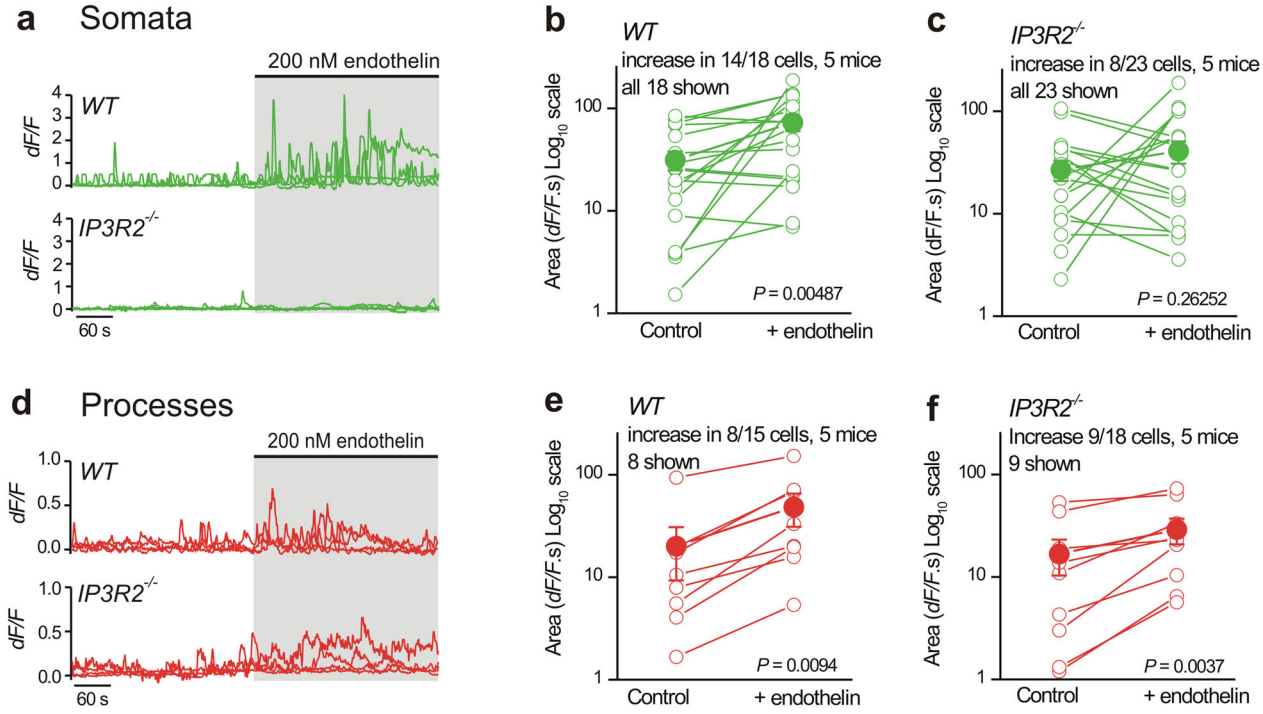

Figure 4. GPCR-mediated Ca^{2+} fluctuations in astrocyte processes are largely intact in hippocampal slices from *IP3R2*$^{-/-}$ mice

a–c. Representative traces and average data for endothelin-evoked Ca^{2+} fluctuations in astrocyte somata from *WT* and *IP3R2*$^{-/-}$ mice. d–f. As in a–c, but for astrocyte processes. Five *WT* and five *IP3R2*$^{-/-}$ mice were analyzed for the experiments reported in this figure, and paired Student's *t* tests were used when comparing before and during endothelin application. The data are shown as mean ± s.e.m.

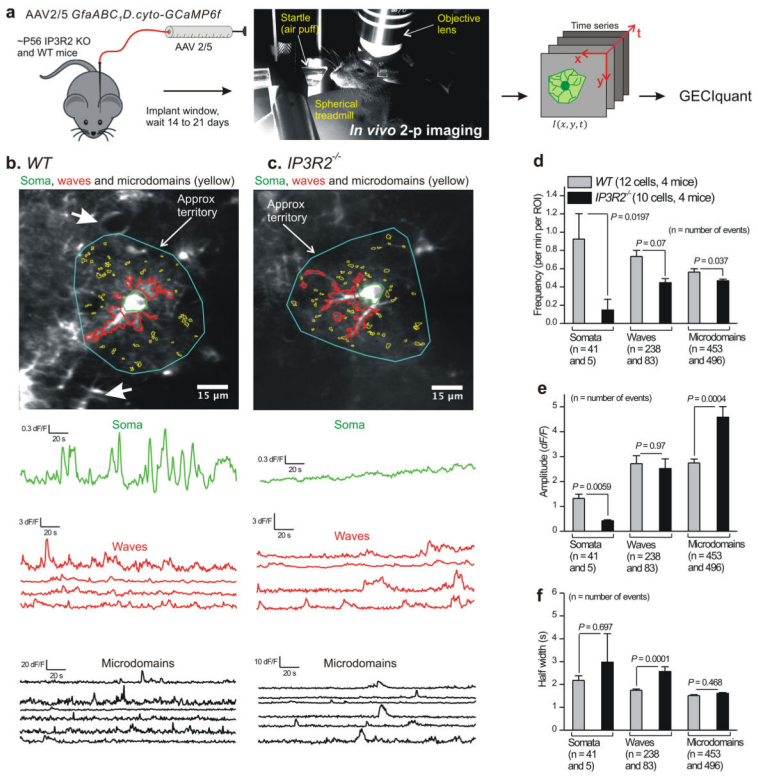

Figure 5. Abundant Ca^{2+} fluctuations persist in astrocyte processes from WT and *IP3R2*$^{-/-}$ mice *in vivo*

a. Schematic illustrating the experimental approach for *in vivo* imaging in fully awake mice free to rest or run on a spherical treadmill (with no anesthesia). **b.** Representative images and traces for Ca^{2+} fluctuations measured in a cortical astrocyte from a *WT* mouse. Three predominant types of Ca^{2+} event are shown: somatic, waves and microdomains. Approximate territory boundaries are outlined in blue, but were not used for data analyses and are shown only for illustrative purposes. **c.** As in b, but for an astrocyte from an *IP3R2*$^{-/-}$ mouse. Representative movies are Supplementary movies 5 and 6. **d–f.** Average data for astrocyte Ca^{2+} fluctuation properties from *WT* and *IP3R2*$^{-/-}$ mice during *in vivo* imaging (n = 12 astrocytes and 4 mice for each). As stated in the figure, the n numbers refer to the numbers of Ca^{2+} fluctuations for each bar, which were averaged for frequency, amplitude and half-width across all cells in panels d–f. The data are shown as mean ± s.e.m.

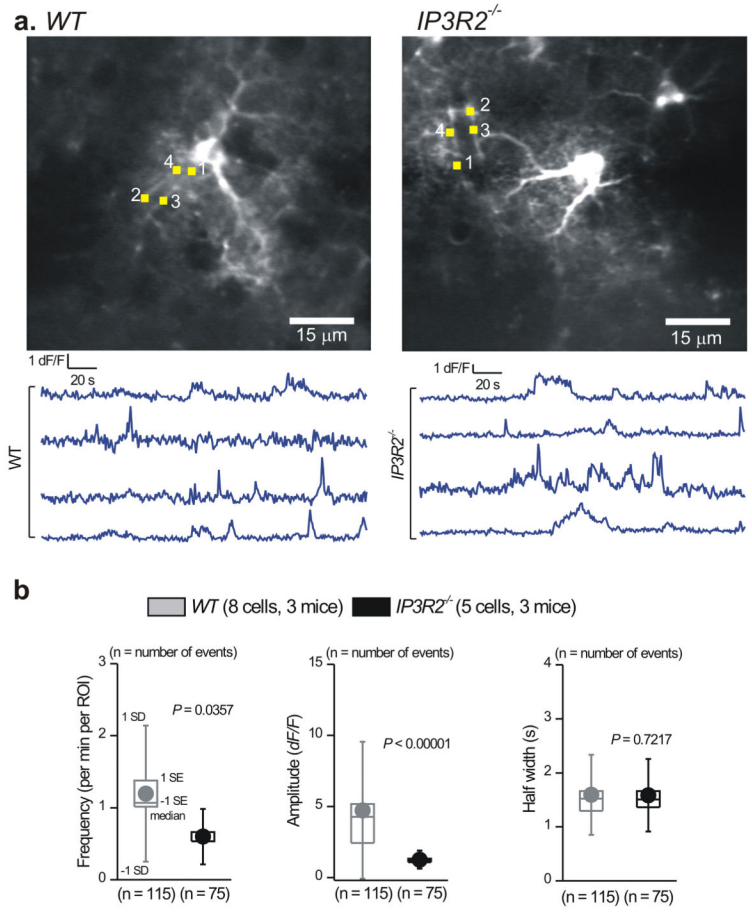

Figure 6. Ca^{2+} fluctuations persist *in vivo* within endfeet of cortical astrocytes from *IP3R2*$^{-/-}$ mice

a. Representative traces and images for Ca^{2+} fluctuations measured in astrocyte endfeet from *WT* and *IP3R2*$^{-/-}$ mice. **b.** Average data for astrocyte Ca^{2+} fluctuation properties from *WT* and *IP3R2*$^{-/-}$ mice during *in vivo* imaging (*WT*: n = 7 astrocytes and 3 mice, *IP3R2*$^{-/-}$: n = 5 astrocytes and 3 mice). The averages are across all cells and are shown as box and whisker plots.

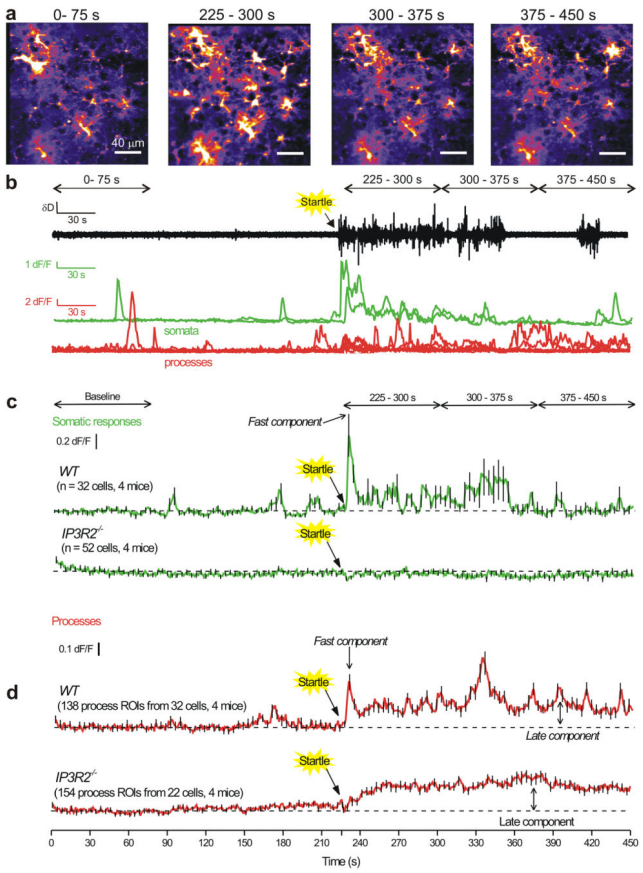

Figure 7. Endogenously evoked astrocyte process Ca^{2+} fluctuations recorded during *in vivo* startle responses reveal early and late components

a. Representative images of Ca^{2+} fluctuations from cortical astrocytes before, during and after startle responses, which were evoked by a puff of air to the face of the mouse (see Methods and Supplementary movie 9). The times written above each of the images correspond to the times shown in the traces in panel b and c. Startle was evoked at 225 s. Representative data for *WT* and *IP3R2*$^{-/-}$ are shown in Supplementary movie 7 and 8. **b**. Representative traces for the animal's locomotion on the spherical treadmill along with Ca^{2+} responses of cortical astrocytes for somatic and process fluctuations for the cells shown in a. Note that startle-triggered running of the mouse on the ball, as well as Ca^{2+} fluctuations in cortical astrocytes. c. Average data for experiments such as those in b for 32 cells from four *WT* and 52 cells from four *IP3R2*$^{-/-}$ mice. d. As in c, but for astrocyte process fluctuations. Note that the responses in the territory displayed a fast/early component and a slow/late component that persisted during these recordings. In the interests of clarity, error bars in panels c and d are shown for every 5th data point, but the underlying average traces are for all cells. The data are shown as mean ± s.e.m.

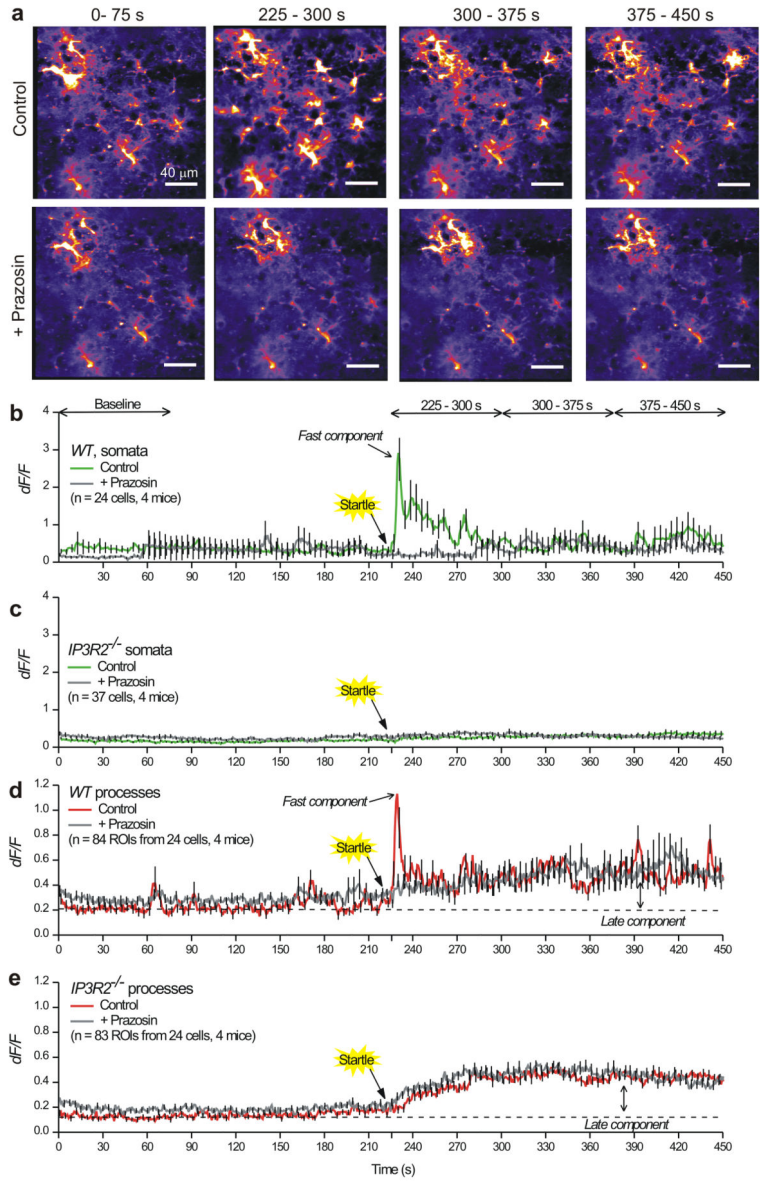

Figure 8. Prazosin-sensitive and insensitive components of the endogenously evoked astrocyte process Ca^{2+} fluctuations recorded during *in vivo* startle responses

a. Representative images of Ca^{2+} fluctuations from cortical astrocytes before, during and after startle responses. The upper panels show control responses to startle without prazosin influence, whereas the lower panels show the same field of view after 1 mg/kg prazosin was injected ip. Startle was evoked at 225 s. Representative data for *WT* are shown in Supplementary movie 8 and 9. **b**. Average traces showing Ca^{2+} responses in cortical astrocytes for somatic Ca^{2+} fluctuations before and after prazosin injections. Note that startle triggered a robust Ca^{2+} response in the somata, that was blocked by prazosin. **c**. Similar experiments to those shown in b, but for astrocytes from *IP3R2*$^{-/-}$ mice. Note that startle evoked no somatic responses. **d**. As in b, but for astrocyte process Ca^{2+} fluctuations. Note that the responses in the processes displayed a fast component with a peak at ~3 s after startle, and a late component that persisted during these recordings. Prazosin blocked only

the fast component. **e**. As in d, but for *IP3R2*$^{-/-}$ mice. The slow component of the Ca^{2+} response triggered by startle was present in the *IP3R2*$^{-/-}$ mice and was insensitive to prazosin. The results shown in this figure are from 4 *WT* and 4 *IP3R2*$^{-/-}$ mice. In the interests of clarity, error bars in panels **b–e** are shown for every 5th data point, but the underlying average traces are for all cells. The data are shown as mean ± s.e.m.